# Sodalite-like carbon based superconductors with Tc about 77 K at ambient pressure

Journal Name

ARTICLE TYPE

Cite this: DOI: 00.0000/xxxxxxxxxx

# Sodalite-like carbon based superconductors with $T_c$ about 77 K at ambient pressure

Siyu Jin,[a‡] Xiaoyu Kuang,[a‡] Xilong Dou,[a] Andreas Hermann,[*b] and Cheng Lu[*c]

Received Date
Accepted Date

DOI: 00.0000/xxxxxxxxxx

The attainment of superconductivity at room temperature is a longstanding aspiration for both experimental and theoretical scientists. Materials exhibiting superconductivity under ambient conditions would possess significant applications. Here, we report two metastable phases of sodalite-like carbon based superconductors, $GaC_6$ and $GeC_6$, at ambient pressure by CALYPSO structural search method and first-principles calculations. Our calculations reveal that both $GaC_6$ and $GeC_6$ compounds are $Im\bar{3}m$ symmetry and dynamically stable at ambient pressure with $T_c$ values up to the boiling point of liquid nitrogen. The underlying mechanisms indicate the guest Ga and Ge atoms serve the dual role in enhancing the structural stability and concurrently acting as electron donors, thereby modulating the electronic properties of the $C_{24}$ covalent frameworks, i.e. from insulating states to superconducting states. The present results offer insights into the exploration of novel high temperature superconductors at ambient conditions.

## 1 Introduction

Since Onnes firstly observed the superconductivity in solid mercury[1], it has commanded sustained attention within the scientific community[2–4]. In the subsequent decades, superconductivity was observed in numerous other materials. In 1913, the superconducting state was identified in lead with $T_c$ of 7 K, while in 1941, niobium nitride was demonstrated to be superconductor at 16 K. Great efforts have been dedicated to the pursuit of superconductivity at increasing temperatures, with the ultimate objective of achieving the room-temperature superconductor. An enormous step forward was the discovery of unconventional superconductivity in the cuprates, which allowed to construct devides cooled by liquid nitrogen[5,6]. Recently, conventional phonon-mediated superconductors have made tremendous progress[7–25]. As the light-element compound, the sulfur hydride, namely $H_3S$, is confirmed to be a superconductor with extremely high $T_c$ value of 203 K at high pressures[25]. Subsequently, hydrogen-rich clathrates in rare earth hydrides were discovered to exhibit ultra-high $T_c$ superconductivity due to the strong electron-phonon coupling (EPC), which is related to the motions of H atoms within the cages and the larger electron densities contributed by H atoms at the Fermi level[26–28]. However, the endeavors to synthesize these superhydrides are constrained by the current technological capabilities. Consequently, the strategies for procuring high $T_c$ superconductors under moderated pressures have garnered widespread attention[29].

The clathrate motif of atomic hydrogen is unlikely to persist at low or ambient pressure. Stronger bound clathrate cages offer more promising routes towards ambient pressure stability. In fact, some non-hydrogen clathrates connected by $sp^3$ hybridized C-C covalent bonds also exhibit superconductivity at moderate or even ambient pressure. Typically, Fullerene ($C_{60}$) is considered to be a semiconductor at ambient conditions and the energy gap is approximately 1.6 eV to 1.7 eV[30]. However, when doped with appropriate atoms, such as alkali metals, fullerenes can become conductive or even exhibit superconductivity[31–33]. The corresponding $T_c$ values increase with the cell volume of alkali metal doped fullerenes. Under ambient conditions, the $T_c$ of $RbCs_2C_{60}$, characterized by a face-centered-cubic structure, is found to be 33 K[31], which is the highest $T_c$ value among the trivalent alkali metal doped fullerenes ($A_3C_{60}$)[31,32]. In contrast, the doped fullerene of $Cs_3C_{60}$, notable for its non-cubic crystalline arrangement, does not exhibit superconductivity under ambient pressure. Interestingly, when $Cs_3C_{60}$ transforms into a cubic structure at high pressure, its $T_c$ reaches to 40 K at 15 kbar[33]. Similarly, the face-centered cubic (FCC) $C_{34}$ clathrate transforms from an insulating state to a metallic state after the intercalations of fluorine atoms, which introduces hole carriers into the top va-

[a] Institute of Atomic and Molecular Physics, Sichuan University, Chengdu 610065, China.
[b] Centre for Science at Extreme Conditions and SUPA, School of Physics and Astronomy, University of Edinburgh, Edinburgh EH9 3FD, United Kingdom. E-mail: a.hermann@ed.ac.uk
[c] School of Mathematics and Physics, China University of Geosciences (Wuhan), Wuhan 430074, China. E-mail: lucheng@calypso.cn

† Electronic Supplementary Information (ESI) available: phonon dispersion curves, bond length, Bader charge, COHP calculations, electronic band structures and densities of states, and EPC calculations of $XC_6$ compounds. See DOI: 00.0000/00000000.

‡ S.-Y. J. and X. -Y. K. contributed equally to this work.

lence bands of the host carbon frameworks. The fluorine-doped carbon clathrate ($FC_{34}$) is predicted to exhibit high temperature superconductivity with a $T_c$ value of 77 K at ambient pressure[34]. Thus, the lattice arrangement with cubic or approximate cubic symmetry, denotes as a pivotal determinant in the pursuit of relatively high $T_c$ values, potentially providing novel avenues for the discovery of high temperature superconductors at ambient conditions.

Recent computational studies have explored the superconducting behaviors of mixed boron-carbon based clathrates at ambient pressure[35], a class of materials that has been shown to be recoverable following high-pressure synthesis[36]. Interestingly, the $T_c$ values of these binary-guest configurations are adjustable through the manipulations of the guest metal atoms, which are attributed to the rigid band behaviors of the $sp^3$ hybridized B-C covalent frameworks in boron-carbon clathrates. Pure carbon clathrates are arguably simpler materials, but have not been synthesized yet. However, they have been studied computationally, including doping with simple metal ions (akin to the fullerene superconductors)[37,38]. Most importantly, the sodalite-like $NaC_6$ is predicted to be a superconductor with high $T_c$ value[39]. A systematic study of this family of materials is still missing. This inspired us to further explore the superconductivities and underlying mechanisms of $sp^3$-bonded $C_6$ clathrates with different guest atoms. In the present work, we carry out systematic high-throughput density functional theory (DFT) calculations to search for the stable $sp^3$-bonded $C_6$ clathrates at ambient pressure and then determine their electronic and superconducting properties. Phonon calculations show that many $XC_6$ compounds (X = Ni, Cu, Zn, Ga, Ge, As, Se, Br, Ru, Rh, Pd, Ag, Cd and I) with $Im\bar{3}m$ symmetry are dynamically stable, including guest atoms ranging from transition metals via $p$-block elements to the halogens (See Fig. S1). Among them, the substantial charge transfers in $GaC_6$ and $GeC_6$ clathrates are observed due to the interactions between metal Ga/Ge atoms and $C_{24}$ cages, which the respective values are 0.12 $e$ and 0.13 $e$ per C atom. The electron phonon coupling (EPC) calculations reveal that $GaC_6$ exhibits a $T_c$ value of 82 K, while $GeC_6$ demonstrates a $T_c$ value of 76 K.

## 2 Computational details

The high-throughput structural searches of carbon based clathrates at ambient pressure are conducted through CALYPSO[40,41] method and density functional theory (DFT) calculations. The crystal structure searches for $GaC_6$ ranging from 1 to 4 f.u./cell have been performed at ambient pressure. Over 5,000 structures have been generated in total. The structural optimizations and the phonon dispersion curve are calculated by the Vienna Ab initio Simulation Package (VASP) package[42–44]. The cutoff energy is chosen as 600 eV and the smallest allowed spacing is chosen as 0.2 $Å^{-1}$ between k points. In addition, tighter setting parameters are used for the phonon mode simulations[45]. EPC calculations are performed by the QUANTUM ESPRESSO code[46] based on the density functional perturbation theory (DFPT). Ultrasoft pseudopotentials of Perdew-Burke-Ernzerhof formula are adopted to calculate the EPC interactions. The cutoff energy and the charge density cutoff are chosen as 100 Ry and 1000 Ry after the convergence test, respectively. The EPC calculations employ a q-mesh of 6 × 6 × 6 in the first Brillouin zone. A k-mesh of 24 × 24 × 24 was used to ensure the sampling of k-points achieved convergence. Taking into account the significant difference in atomic mass between carbon and metal atoms, Gor'kov and Kresin (G-K) divide the phonon spectrum into two regions: optical and acoustic phonons. We can introduce the the coupling constants $\lambda_{opt}$ and $\lambda_{ac}$ to characterize the relative contribution of the acoustic and optical branches to the total electron-phonon coupling strength[47,48]. In common metals, the function $\alpha^2F(\omega)$ is characterized by a peak in the phonon density of states. Such fact permits the replacement of $\omega(\mathbf{q})$ in the phonon propagator by its average value $\tilde{\omega}^2 = <\omega^2>^{1/2}$. At $T = T_c$, the order parameter can be written as:

$$\Delta(\omega_n)Z = \pi T \sum_m \left[ \frac{\tilde{\omega}_{opt}^2}{(\omega_n-\omega_m)^2+\tilde{\omega}_{opt}^2} \times (\lambda_{opt}-\mu^*) + \frac{\tilde{\omega}_{ac}^2}{(\omega_n-\omega_m)^2+\tilde{\omega}_{ac}^2} \times \lambda_{ac} \right] \frac{\Delta\omega_m}{\omega_m} \tag{1}$$

the electron-phonon coupling $\lambda$ is given by

$$\begin{aligned} \lambda &= \lambda_{opt} + \lambda_{ac} \\ &= 2\int_0^{\omega_{amax}} \frac{\alpha^2F(\omega)}{\omega} d\omega + 2\int_{\omega_{amax}}^{\omega_{omax}} \frac{\alpha^2F(\omega)}{\omega} d\omega \end{aligned} \tag{2}$$

In Eq. 2, the $\omega_{amax}$ and $\omega_{omax}$ represent the maximum frequency of acoustic and optical models, respectively. Here, it is defined as follows:

$$\begin{aligned} <\omega_{ac}^2> &= \frac{2}{\lambda ac}\int_0^{\omega_{amax}} \omega^2 \frac{\alpha^2F(\omega)}{\omega} d(\omega) \\ &= \frac{2}{\lambda ac}\int_0^{\omega_{amax}} \omega \times \alpha^2F(\omega) d(\omega) \end{aligned} \tag{3}$$

$$\begin{aligned} <\omega_{opt}^2> &= \frac{2}{\lambda opt}\int_{\omega_{amax}}^{\omega_{omax}} \omega^2 \frac{\alpha^2F(\omega)}{\omega} d(\omega) \\ &= \frac{2}{\lambda opt}\int_{\omega_{amax}}^{\omega_{omax}} \omega \times \alpha^2F(\omega) d(\omega) \end{aligned} \tag{4}$$

In case $\lambda_{ac} << \lambda_{opt}$, and assuming that:

$$T_c = T_c^{opt} + \Delta T_c^{ac}, \quad and \quad T_c^{opt} >> \Delta T_c^{ac} \tag{5}$$

the $T_c$ can be identified by using the following equation:

$$\begin{aligned} T_c &= \left[ 1 + 2\frac{\lambda_{ac}}{\lambda_{opt}-\mu^*} \times \frac{1}{1+\rho^{-2}} \right] T_c^0, \\ \rho &= \frac{\tilde{\omega}_{ac}}{\pi T_c^0}, \quad T_c^0 \equiv T_c^{opt} \end{aligned} \tag{6}$$

where ${T_c}^0$ is the transition temperatures contributed by the the coupling between the electrons and the optical models. For $\lambda_{opt} \leq 1.5$, it is defined as follows:

$$T_c^0 = \frac{\tilde{\omega}_{opt}}{1.2} exp\left[ -\frac{1.04(1+\lambda_{opt})}{\lambda_{opt}-\mu^*(1+0.62\lambda_{opt})} \right] \tag{7}$$

**Table 1** Calculated EPC parameters and $T_c$ of $GaC_6$ and $GeC_6$ at ambient pressure. The Mc-A-D, G-K and IE correspond to the $T_c$ obtained by the Allen-Dynes modified McMillan equation, the Gor'kov and Kresin equation and the isotropic Eliashberg equation, respectively. The units of $\omega_{log}$, and $T_c$ are Kelvin ($K$).

| | $\lambda_{ac}$ | $\lambda_{opt}$ | $\lambda$ | $\omega_{log}$ | $f_1{*}f_2$ | Mc-A-D | G-K | IE |
|---|---|---|---|---|---|---|---|---|
| $GaC_6$ | 0.17 | 1.26 | 1.44 | 616.30 | 1.10 | 75 | 82 | 87 |
| $GeC_6$ | 0.32 | 1.11 | 1.47 | 649.38 | 1.11 | 60 | 76 | 69 |

For $\lambda_{opt}$>1.5 , it is given by:

$$T_c^0 = \frac{0.25\tilde{\omega}_{opt}}{\left[e^{\frac{2}{\lambda_{eff}}} - 1\right]^{1/2}} \tag{8}$$

where $\lambda_{eff}$is given by:

$$\begin{aligned} \lambda_{eff} &= (\lambda_{opt} - \mu^*)\left[1 + 2\mu^* + \lambda_{opt}\mu^* t(\lambda_{opt})\right]^{-1} \\ t(x) &= 1.5exp(-0.28)x \end{aligned} \tag{9}$$

## 3 Results and discussions

Fig. 1(a) depicts the crystal structure of $GaC_6$ at ambient pressure. The host carbon clathrate displays a structural composition comprising six square C4 rings and six hexagonal C6 rings, resembling the structure of sodalite. The guest Ga atoms are located at the center of cubic unit, forming a body-centered cubic structure with $Im\bar{3}m$ symmetry. Table S1 summarizes the C-C and Ga-C bond lengths of $GaC_6$. Specifically, the C-C bond lengths in $GaC_6$ are 1.640 , while the Ga-C bond lengths are 2.593 . The C-C bond length is significantly elongated compared to the pure C-sodalite (no guest), where it is 1.543 .

Fig. 1(b) illustrates the electron localization functions (ELF)[49,50] of $GaC_6$. It can be seen that the valence electrons of the C atoms are primarily localized on the C-C bonds, forming strong covalent $\sigma$ bonds. In contrast, the valence electrons of the guest Ga atoms are concentrated near the atoms. This phenomenon indicates that in $GaC_6$, each C atom is linked to other four carbon atoms through $sp^3$ hybridized covalent bonds, creating two types of bond angles: 90° and 120° (e.g., ∠C2-C1-C3 and ∠C3-C1-C4). Meanwhile, the guest Ga atoms are encapsulated in the C cages with weak interactions between Ga atoms and C atoms. However, the guest atoms play a pivotal role in buttressing the structures and wield the capacity to regulate the electrons of $C_{24}$ covalent frameworks.

The Bader charges[51] of the $GaC_6$ indicate a slight charge transfer between the guest Ga atoms and the C atoms. Each C atom accepts about 0.12 $e$ from the guest atom, indicating that the C atoms act as the electron acceptors in $GaC_6$, since each C atom forms a strong covalent bond with four adjacent C atoms, and the four valence electrons of the C atom are firmly bound within the $C_{24}$ cage.

The analysis of Crystal Orbital Hamilton Population (COHP) analysis[52,53] for $GaC_6$ is depicted in Fig. S2 and Table S1 . The negative projected COHP (-pCOHP) and the negative integrated COHP (-ICOHP) of both Ga-C and covalent C-C pairs are presented. The -ICOHP values of C-C bonds are 7.44 eV/atom pair, an order of magnitude higher than those of Ga-C bonds (0.61 eV/atom pair), suggesting that the C-C bonds are considerably stronger than the Ga-C bonds, in agreement with the above ELF results. It can be seen from Fig. S2 that the Ga-C bonds in $GaC_6$ exhibit almost no anti-bonding states below the Fermi level, which is beneficial to the stability of the structure. In contrast, for example in the $AgC_6$ and $NiC_6$ compounds, the regions of the $d$ orbitals of Ag and Ni atoms contributing to the density of states show visibly anti-bonding states, indicating that the aggregation of energy bands contributed by the $d$ orbitals of transition metal atoms is detrimental to the stabilities of the compounds (See Fig. S3).

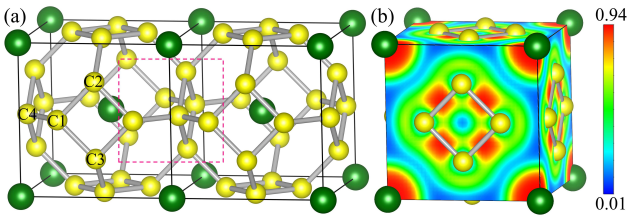


**Fig. 1** (a) Crystal structure of $XC_6$, the X and C atoms are represented by green and yellow balls, respectively. (b) The periodic table of $T_c$ values for $XC_6$.

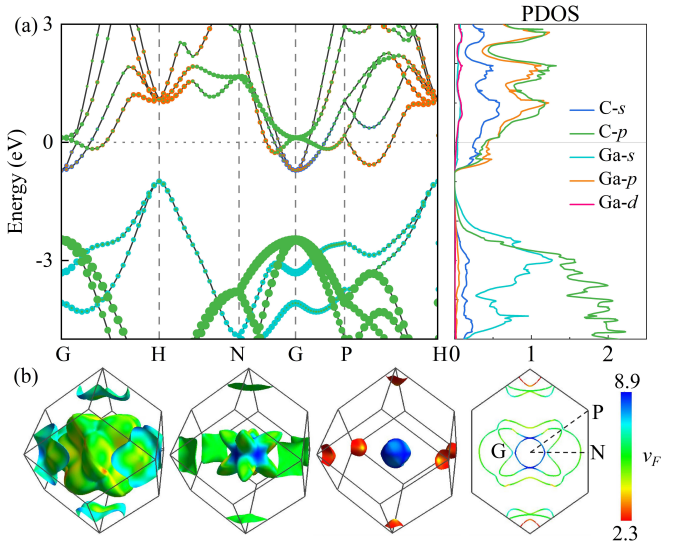


**Fig. 2** (a) The calculated electronic band structure and projected DOS (PDOS) for $GaC_6$. (b) Fermi surface sheets of $GaC_6$.

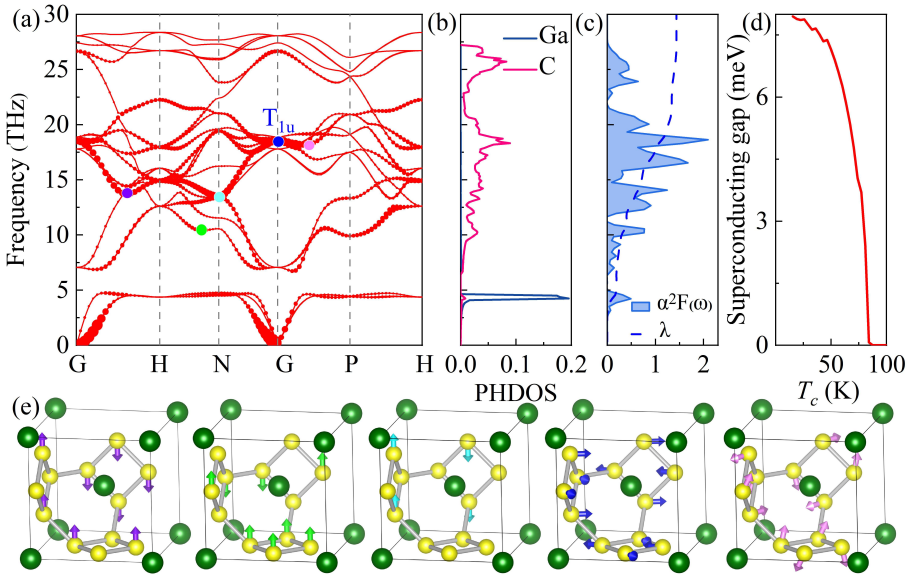


**Fig. 3** (a)-(d) Calculated phonon dispersion (the radius of the red circle is proportional to the phonon linewidth), projected phonon density of states (PHDOS), Eliashberg phonon spectral function $\alpha^2F(\omega)$, integrated EPC $\lambda(\omega)$ and calculated superconducting gap for $GaC_6$ at ambient pressure. (e) Vibration patterns for purple point, green point, azure point, blue point ($T_{1u}$ phonon mode at Gamma point) and pink point, respectively.

To gain further insights into the electronic properties of the $GaC_6$, we perform the electronic band structure, projected electronic density of states (PDOS), Fermi surfaces and EPC calculations. The results are shown in Fig. 2. The band structure visualizes the electron doping from Ga into the C-sublattice. The latter exhibits a sizeable gap between bonding and antibonding states of C-$s$ and C-$p$ character. The Ga 4$s$ states are in the occupied/valence region, while the donation of the Ga 4$p$ electron into the C-sublattice leads to partial occupancy of the antibonding C-$sp^3$ states and therefore metallic character. The electronic DOSs at the Fermi level ($N(E_f)$) of $GaC_6$ are primarily contributed by C-$s$, C-$p$ and Ga-$p$ states. Notably, the aggregate contributions of C-$s$ and C-$p$ states are more than half of the total DOS, which suggests the possibility of strong EPC and the prospect of high temperature superconductivity[54]. We further calculate the projected DOS for Ga $d$-orbitals. As shown in Fig. S4, the $d_{x^2}$ orbital states of Ga atoms predominate around the Fermi level, exhibiting several peaks. In contrast, the distribution of other $d$ orbitals of Ga atoms is more diffuse, with lower contribution. The Fermi surfaces of $GaC_6$ are displayed in Fig. 2(b), indicating three electron pockets around Gamma point. One is very small and the other two are large with multiple bulges. We then calculate the Eliashberg spectral function $\alpha^2F(\omega)$ of $GaC_6$, which enabled us to obtain the EPC parameters through a straightforward frequency domain integration. The results reveal that the EPC parameter $\lambda$ of $GaC_6$ at ambient pressure is 1.44, which is larger than the value of 0.7 for $MgB_2$[19]. The superconducting critical temperatures are estimated by solving the Allen-Dynes modified McMillan (Mc-A-D) equation[55], the Gor'kov and Kresin (G-K) equation[47,48] and the isotropic Eliashberg (IE) equation[56] (See Table 1). These comprehensive approaches are employed to derive a judicious range of $T_c$ values. Using the Gor'kov and Kresin equation, we estimate the $T_c$ to be 82 K ($\mu^* = 0.1$). Thus, we conduct further analyses of the band structures to find the superconductivity mechanism of $GaC_6$. Fig. 2(a) illustrates the abundance of electronic states in close proximity to the Fermi level, which elucidate that multiple energy bands crossing through it. The energy bands that cross through the Fermi level at the Gamma point are relatively flat, implying that the Fermi velocities approach to zero. These flat bands hold the potentials to significantly increase the electronic density of states at the Fermi level. Along N-G-P line, the energy bands crossing the Fermi level in this region are steep, which indicate the large gradients corresponding to high conduction electron velocities[54]. The significant difference in electron velocities at the Fermi level, attributed to the coexistence of energy bands of flat and steep profiles passing through the Fermi level, serves as the catalyst for enhancing the EPC, which is similar to the superconducting mechanism observed in $MgB_2$[57,58].

To gain a deeper understanding of the superconductivity of $GaC_6$, we perform calculations of the phonon dispersion curves, phonon density of states (PHDOS), Eliashberg phonon spectral function $\alpha^2F(\omega)$, and integrated EPC $\lambda(\omega)$ (See Fig. 3). The strength of the EPC at given wave vectors and modes $\lambda_{qv}$ is indicated by the red circles in phonon dispersion curves. Based on the phonon dispersion curves of $GaC_6$, as shown in Fig. 3(a), a small gap is observed between 4.6 THz and 6.4 THz. The phonon modes below the gap are predominantly contributed by Ga atoms. These are dispersionless "rattling" modes of the Ga atom in the cage, leading - as can be clearly seen from Fig. 3(b) - to a sharp peak in the PHDOS at 4.23 THz. The phonon modes above the gap are mostly contributed by C atoms. From Fig. 3(c), it is evident that the medium frequency regions (4.9 THz -22.2 THz) contribute significantly to the EPC, accounting for 79% of the total $\lambda_{qv}$. The superconducting gap of $GaC_6$ is displayed in Fig. 3(d), indicating that the $T_c$ value of $GaC_6$ is about 87 K under ambient pressure. Interestingly, the $T_{1u}$ phonon mode, character-

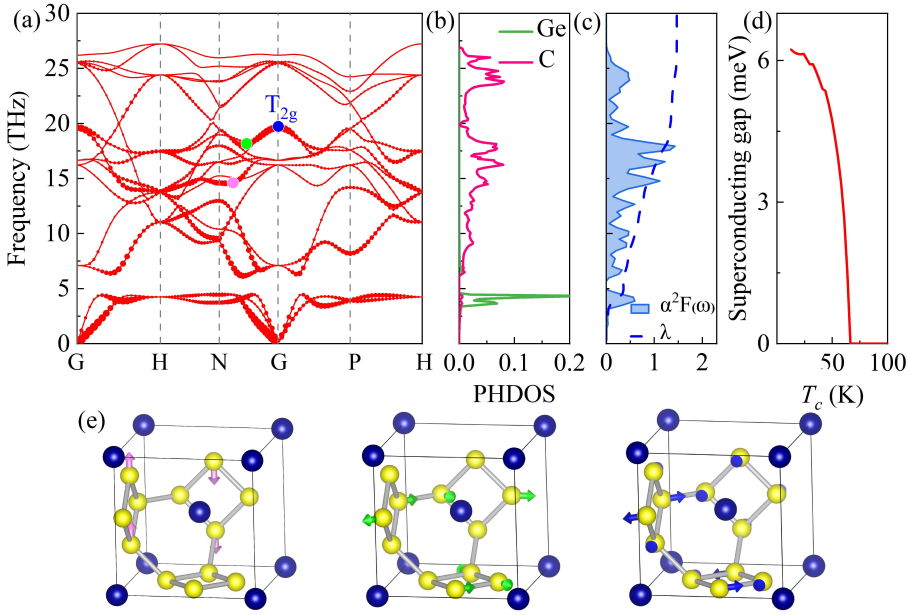


**Fig. 4** (a)-(d) Calculated phonon dispersion (the radius of the red circle is proportional to the phonon linewidth), projected phonon density of states (PHDOS), Eliashberg phonon spectral function $\alpha^2F(\omega)$, integrated EPC $\lambda(\omega)$ and calculated superconducting gap for $GeC_6$ at ambient pressure. (e) Vibration patterns for pink point, green point and blue point ($T_{2g}$ phonon mode at Gamma point), respectively.

ized by a triple degeneracy and located at Gamma point, exhibits significant softening and possesses the highest $\lambda_{qv}$ value and a relatively high frequency (about 18 THz), coupling strongly with electrons. The displacement vector of the $T_{1u}$ phonon mode reveals that the Ga atoms in $GaC_6$ are relatively inert. Meanwhile, the vibrations of the adjacent C atoms in $C_{24}$ frameworks strongly stretch the $\sigma$ bonds between them. Thus, the $T_{1u}$ mode is a three dimensional $\sigma$-bond stretching optical mode. In addition to the $T_{1u}$ mode, several other phonon modes with significant softening are also observed, including the phonon mode along the H-N line near 10 THz, the phonon mode along the G-H line near 13 THz, the phonon mode at the N point near 13 THz, and the phonon mode along the G-P line near 17 THz, as shown in Fig. 3(e). These modes correspond to several main peaks of $\alpha^2F(\omega)$, indicating their crucial roles in the EPC interactions. Finally, the phonon modes contributed by C atoms in the high frequency regions contribute about 8% to the EPC.

We now discuss the stability of $Im\bar{3}m$-$GaC_6$ compound. We performed enthalpy calculations for the $Im\bar{3}m$-$GaC_6$ across the pressure range of 0 to 80 GPa, including possible decomposition reactions. As shown in Fig. S5, the $Im\bar{3}m$-$GaC_6$ was found to have higher enthalpy than the elemental assemblage of diamond and gallium at ambient pressure. The higher energy may stem from strained $sp^3$ bonds within the sodalite cage. As the pressure increases, the assemblage of $C_{60}$ and gallium would be a potential synthesis route to reach the $Im\bar{3}m$-$GaC_6$ at 60 GPa. According to previous studies, $SrB_3C_3$, possessing a similarly strong covalent structure as $GaC_6$, has been synthesized at near 50 GPa and quenched to ambient conditions in an inert atmosphere[36,59]. Thus, by analogy to other covalent bonded structures that are formed under pressure, these materials may allow metastable persistence at ambient conditions.

$GeC_6$ compound is another sodalite-like carbon based superconductor with $T_c$ value of 76 K ($\mu^* = 0.1$) at ambient pressure, which is probably not too surprising given that Ga and Ge are adjacent in the periodic table with similar atomic size and covalent radius[60]. Their electron count differs however, and as consequence $GeC_6$ exhibits the highest charge transfer in this study with approximately 0.8 $e$ per Ge atom, but the contributions of Ge-$p$ orbitals at the Fermi level are significant. Additionally, the bands crossing the Fermi level are relatively steep, without the presence of flat band (See Fig. S6). In $GeC_6$, the conduction band minimum crosses the Fermi level, indicating that $GeC_6$ is also an electron-doped conductor. As shown in Fig. 4, the Ge atom primarily contributes to the dispersionless rattling modes in the low frequency region, contributing approximately 24% to the EPC. The medium frequency region accounts for 69% of the total $\lambda$ value contributing to the EPC in $GeC_6$. The most significant contributor to the EPC in the medium frequency region is the $T_{2g}$ phonon mode located at the Gamma point with a frequency of approximately 19.6 THz. Specifically, the $T_{2g}$ phonon mode is mainly contributed by C atoms. Except for the $T_{2g}$ mode, there are two additional phonon modes that exert notable influence on the $\lambda$ value, accompanied by observable softening. These modes are identified as follows: the phonon mode along the N-G direction, approximately located at 14.5 THz, and another phonon mode along the same N-G direction, positioned around 17.6 THz (See Fig. 4). These two modes, in conjunction with the $T_{2g}$ mode, correspond to several prominent peaks of $\alpha^2F(\omega)$, implying their crucial contributions to the EPC and $T_c$ of 76 K at ambient pressure.

A series of other $XC_6$ compounds (X = Ni, Cu, Zn, Ga, Ge, As,

Se, Br, Ru, Rh, Pd, Ag, Cd and I) with $Im\bar{3}m$ symmetry are found to be dynamically stable at ambient pressure (See Fig. S1). All compounds other than $PdC_6$, a semiconductor with a band gap of 0.2 eV, are metallic. Tables S2 and S3 summarize the density of states at the Fermi level for each compound, as well as partial charges and predicted $T_c$. The $T_c$ values for these compounds are lower than those observed in $GaC_6$ and $GeC_6$, ranging from 5 to 30 K. The changes in EPC will depend on guest atom mass but also on the extent of charge transfer and nature of the electronic states at the Fermi level. The free electrons of the C atoms in the $C_{24}$ cages form $sp^3$ covalent bonds with the other four C atoms, so those electrons are bound within the chemical bonds and cannot participate in conduction. As a result, the pure carbon cage is an insulator, similar to diamond. For more electronegative guest species, the halogens Br and I, the $N(E_f)$ is high: in $BrC_6$ it is the highest among all $XC_6$ compounds, reaching 11.84 states/eV/cell. But the Br atom transfers only 0.08 $e$ to the $C_{24}$ cage, which is insufficient to provide enough electrons for the $C_{24}$ cage, resulting in a low $T_c$ of 5 K. For transition metals, $N(E_f)$ can also be high, for example in $NiC_6$ the $N(E_f)$ is 10.87 states/eV/cell, but the electronic DOSs at the Fermi level predominantly originate from Ni-$d$ orbitals (See Fig. S3). The calculated $T_c$ value of $NiC_6$ compound is 13 K, implying that partially filled $d$-shells and therefore an abundance of X-$d$ states at the Fermi level may not be promising for strong EPC and the potential for superconductivity. This is similar to the situation in lanthanide superhydrides[21].

## 4 Conclusions

In summary, we employ high-throughput DFT calculations to investigate sodalite-like carbon based superconductors at ambient pressure for a wide range of potential guest atom species. Two $sp^3$-bonded $C_{24}$ clathrates of $GaC_6$ and $GeC_6$ are found to be excellent superconductors with $T_c$ values near to and above the boiling point of liquid nitrogen. The guest Ga and Ge atoms enhance the structural stability of $C_{24}$ cage while concomitantly act as the electron donors, which regulates the electronic properties of the $C_{24}$ covalent frameworks. The calculated results elucidate that the abundance of electronic states contributed by C atoms near the Fermi level and the obvious discrepancies of the electron velocities at the Fermi level, corresponding to the "flat-bands/steep-bands" scenarios, are the key factors to the high temperature superconductivity of $GaC_6$ and $GeC_6$ superconductors. These findings enrich the categories of superconductors at ambient pressure and provide crucial insights for further design and synthesis of novel high temperature superconductors.

## Author contributions

C.L., S.Y.J. and X.Y.K. provied the idea and designed research. S.Y.J. and X.L.D. completed the first-principles calculations. All authors took part in the analysis of results and discussionsof the research. S.Y.J. wrote the manuscrip. X.Y.K., C.L., and A.H. edited the manuscript.

## Conflicts of interest

There are no conflicts to declare.


## Acknowledgements

This work is supported by the National Natural Science Foundation of China (Grant No. 12174352 and 11874043), the Royal Society International Exchange Scheme (Grant No. IEC\NSFC\201359) and the Fundamental Research Funds for the Central Universities, China University of Geosciences (Wuhan) (Grant No. G1323523065).


## Notes and references


1 H. Kamerlingh Onnes, *Proc. R. Neth. Acad. Arts Sci.*, 1911, **13**, 1093–1113.

2 G. Aschermann, E. Friederich, E. Justi and J. Kramer, *Physik Z.*, 1941, **42**, 349–360.

3 J. Eisenstein, *Rev. Mod. Phys.*, 1954, **26**, 277–291.

4 Y.-L. Hai, M.-J. Jiang, H.-L. Tian, G.-H. Zhong, W.-J. Li, C.-L. Yang, X.-J. Chen and H.-Q. Lin, *Adv. Sci.*, 2023, 2303639.

5 J. G. Bednorz and K. A. Muller, *Z. Phys. B: Condens. Matter*, 1986, **64**, 189–193.

6 C. Proust and L. Taillefer, *Annu. Rev. Condens. Matter Phys.*, 2019, **10**, 409–429.

7 T. Gu, W. Cui, J. Hao, J. Shi and Y. Li, *J. Mater. Chem. C*, 2023, **11**, 6386–6392.

8 S. Zhang, R. A. Susilo, S. Wan, W. Deng, B. Chen and C. Gao, *J. Mater. Chem. C*, 2023, **11**, 12254–12260.

9 X. Zhong, Y. Sun, T. Iitaka, M. Xu, H. Liu, R. J. Hemley, C. Chen and Y. Ma, *J. Am. Chem. Soc.*, 2022, **144**, 13394–13400.

10 Y. Xi, X. Jing, Z. Xu, N. Liu, Y. Liu, M.-L. Lin, M. Yang, Y. Sun, J. Zhuang, X. Xu, W. Hao, Y. Li, X. Li, X. Wei, P.-H. Tan, Q. Li, B. Liu, S. X. Dou and Y. Du, *J. Am. Chem. Soc.*, 2022, **144**, 18887–18895.

11 M. Rahm, R. Hoffmann and N. W. Ashcroft, *J. Am. Chem. Soc.*, 2017, **139**, 8740–8751.

12 A. P. Drozdov, P. P. Kong, V. S. Minkov, S. P. Besedin, M. A. Kuzovnikov, S. Mozaffari, L. Balicas, F. F. Balakirev, D. E. Graf, V. B. Prakapenka, E. Greenberg, D. A. Knyazev, M. Tkacz and M. I. Eremets, *Nature*, 2019, **569**, 528–531.

13 J. Nagamatsu, N. Nakagawa, T. Muranaka, Y. Zenitani and J. Akimitsu, *Nature*, 2001, **410**, 63–64.

14 H. J. Choi, D. Roundy, H. Sun, M. L. Cohen and S. G. Louie, *Nature*, 2002, **418**, 758–760.

15 K. Sano, Y. Masuda and H. Ito, *J. Phys. Soc. Jpn.*, 2022, **91**, 083703.

16 Z. Tan, H. Zhang, X. Wu, J. Xing, Q. Zhang and J. Zhu, *Phys. Rev. Lett.*, 2023, **130**, 246802.

17 Y. Sun, J. Lv, Y. Xie, H. Liu and Y. Ma, *Phys. Rev. Lett.*, 2019, **123**, 097001.

18 Z. Zhang, T. Cui, M. J. Hutcheon, A. M. Shipley, H. Song, M. Du, V. Z. Kresin, D. Duan, C. J. Pickard and Y. Yao, *Phys. Rev. Lett.*, 2022, **128**, 047001.

19 J. Kortus, I. I. Mazin, K. D. Belashchenko, V. P. Antropov and L. L. Boyer, *Phys. Rev. Lett.*, 2001, **86**, 4656–4659.

20 S. Di Cataldo, S. Qulaghasi, G. B. Bachelet and L. Boeri, *Phys. Rev. B*, 2022, **105**, 064516.

21 W. Sun, X. Kuang, H. D. J. Keen, C. Lu and A. Hermann, *Phys. Rev. B*, 2020, **102**, 144524.

22 B. Chen, L. J. Conway, W. Sun, X. Kuang, C. Lu and A. Hermann, *Phys. Rev. B*, 2021, **103**, 035131.

23 X. Dou, X. Kuang, W. Sun, G. Jiang, C. Lu and A. Hermann, *Phys. Rev. B*, 2021, **104**, 224510.

24 W. Sun, B. Chen, X. Li, F. Peng, A. Hermann and C. Lu, *Phys. Rev. B*, 2023, **107**, 214511.

25 A. P. Drozdov, M. I. Eremets, I. A. Troyan, V. Ksenofontov and S. I. Shylin, *Nature*, 2015, **525**, 73–76.

26 F. Peng, Y. Sun, C. J. Pickard, R. J. Needs, Q. Wu and Y. Ma, *Phys. Rev. Lett.*, 2017, **119**, 107001.

27 Z. M. Geballe, H. Liu, A. K. Mishra, M. Ahart, M. Somayazulu, Y. Meng, M. Baldini and R. J. Hemley, *Angew. Chem. Int. Ed.*, 2018, **57**, 688–692.

28 M. Somayazulu, M. Ahart, A. K. Mishra, Z. M. Geballe, M. Baldini, Y. Meng, V. V. Struzhkin and R. J. Hemley, *Phys. Rev. Lett.*, 2019, **122**, 027001.

29 Y. Song, J. Bi, Y. Nakamoto, K. Shimizu, H. Liu, B. Zou, G. Liu, H. Wang and Y. Ma, *Phys. Rev. Lett.*, 2023, **130**, 266001.

30 Y. Saito, H. Shinohara, M. Kato, H. Nagashima, M. Ohkohchi and Y. Ando, *Chem. Phys. Lett.*, 1992, **189**, 236–240.

31 O. Gunnarsson, *Rev. Mod. Phys.*, 1997, **69**, 575–606.

32 Y. Iwasa and T. Takenobu, *J. Phys.: Condens. Matter*, 2003, **15**, R495.

33 T. T. M. Palstra, O. Zhou, Y. Iwasa, P. E. Sulewski, R. M. Fleming and B. R. Zegarski, *Solid State Commun.*, 1995, **93**, 327–330.

34 F. Zipoli, M. Bernasconi and G. Benedek, *Phys. Rev. B*, 2006, **74**, 205408.

35 N. Geng, K. P. Hilleke, L. Zhu, X. Wang, T. A. Strobel and E. Zurek, *J. Am. Chem. Soc.*, 2023, **145**, 1696–1706.

36 L. Zhu, G. M. Borstad, H. Liu, P. A. Gunka, M. Guerette, J.-A. Dolyniuk, Y. Meng, E. Greenberg, V. B. Prakapenka, B. L. Chaloux, A. Epshteyn, R. E. Cohen and T. A. Strobel, *Sci. Adv.*, 2020, **6**, eaay8361.

37 A. Ker, E. Todorov, R. Rousseau, K. Uehara, F.-X. Lannuzel and J. S. Tse, *Chem. Eur. J.*, 2002, **8**, 2787–2798.

38 N. Rey, A. Munoz, P. Rodriguez-Hernandez and A. S. Miguel, *J. Phys.: Condens. Matter*, 2008, **20**, 215218.

39 S. Lu, H. Liu, I. I. Naumov, S. Meng, Y. Li, J. S. Tse, B. Yang and R. J. Hemley, *Phys. Rev. B*, 2016, **93**, 104509.

40 J. Lv, Y. Wang, L. Zhu and Y. Ma, *J. Chem. Phys.*, 2012, **137**, 084104.

41 Y. Wang, J. Lv, L. Zhu and Y. Ma, *Phys. Rev. B*, 2010, **82**, 094116.

42 J. Hafner, *Comput. Phys. Commun.*, 2007, **177**, 6–13.

43 J. P. Perdew, K. Burke and M. Ernzerhof, *Phys. Rev. Lett.*, 1996, **77**, 3865–3868.

44 G. Kresse and D. Joubert, *Phys. Rev. B*, 1999, **59**, 1758–1775.

45 A. Togo and I. Tanaka, *Scr. Mater.*, 2015, **108**, 1–5.

46 P. Giannozzi, S. Baroni, N. Bonini, M. Calandra, R. Car, C. Cavazzoni, D. Ceresoli, G. L. Chiarotti, M. Cococcioni, I. Dabo, A. D. Corso, S. de Gironcoli, S. Fabris, G. Fratesi, R. Gebauer, U. Gerstmann, C. Gougoussis, A. Kokalj, M. Lazzeri, L. Martin-Samos, N. Marzari, F. Mauri, R. Mazzarello, S. Paolini, A. Pasquarello, L. Paulatto, C. Sbraccia, S. Scandolo, G. Sclauzero, A. P. Seitsonen, A. Smogunov, P. Umari and R. M. Wentzcovitch, *J. Phys.: Condens. Matter*, 2009, **21**, 395502.

47 L. P. Gor'kov and V. Z. Kresin, *Sci. Rep.*, 2016, **6**, 25608.

48 L. P. Gor'kov and V. Z. Kresin, *Rev. Mod. Phys.*, 2018, **90**, 011001.

49 A. D. Becke and K. E. Edgecombe, *J. Chem. Phys.*, 1990, **92**, 5397–5403.

50 A. Savin, O. Jepsen, J. Flad, O. K. Andersen, H. Preuss and H. G. von Schnering, *Angew. Chem. Int. Ed.*, 1992, **31**, 187–188.

51 R. F. W. Bader, *Atoms in Molecules: A Quantum Theory (Oxford University Press, Oxford, 1994)*.

52 R. Dronskowski and P. E. Bloechl, *J. Phys. Chem.*, 1993, **97**, 8617–8624.

53 S. Maintz, V. L. Deringer, A. L. Tchougreeff and R. Dronskowski, *J. Comput. Chem.*, 2013, **34**, 2557–2567.

54 A. Simon, *Angew. Chem. Int. Ed.*, 1997, **36**, 1788–1806.

55 P. B. Allen and R. C. Dynes, *Phys. Rev. B*, 1975, **12**, 905–922.

56 G. M. Eliashberg, *J. Exp. Theor.*, 1960, **11**, 696–702.

57 A. Bussmann-Holder, J. Kohler, M. H. Whangbo, A. Bianconi and A. Simon, *Nov. Supercond. Mater.*, 2016, **2**, 37–42.

58 S. Deng, A. Simon and J. Köhler, *Int. J. Mod. Phys. B*, 2005, **19**, 29–36.

59 L. Zhu, H. Liu, M. Somayazulu, Y. Meng, P. A. Guńka, T. B. Shiell, C. Kenney-Benson, S. Chariton, V. B. Prakapenka, H. Yoon, J. A. Horn, J. Paglione, R. Hoffmann, R. E. Cohen and T. A. Strobel, *Phys. Rev. Res.*, 2023, **5**, 013012.

60 B. Cordero, V. Gomez, A. E. Platero-Prats, M. Reves, J. Echeverria, E. Cremades, F. Barragan and S. Alvarez, *Dalton Trans.*, 2008, 2832–2838.